CHAPTER 5

MODES OF RESONATORS WITH ARBITRARY SMOOTH CONTOURS

As already explained in Chapters 1 and 2, laser microcavity shaped as a circular disk provides exponentially low lasing thresholds of the whispering-gallery modes but the emission on these modes has low directivity of these modes equal to 2. In practical applications, however, it is usually necessary to have a source of light with high directivity of emission that enables one to process optical signals with higher efficiency and using smaller space.

One of the traditional methods of solving this problem is the use of a collimating lens in whose focus a low-directional source of waves is placed. The lens, however, is able to catch the light radiated in a limited sector of angles only. Besides, the use of lens greatly increases the overall dimensions of a light-emitting device. Still however if one makes the lens smaller, then the lens starts behaving as an open passive resonator optically coupled with an active resonator of the source of light. This may lead, as it has been shown in Chapters 3 and 4, to the pulling of the working-mode field into the lens and eventually to the failure of the light-emitting device because of the growth of the lasing threshold.

Therefore it is not a surprise that all groups of researchers engaged in the microlaser research and development are looking for the configurations able to provide a better directionality however keep the low threshold of emission [69–72, 74]. Among the promising modified shapes, they have considered stadium, limacon, square, cut circle, perforated circle and stadium, and others. Still the highest expectations and the largest amount of efforts have been associated with, apparently, a spiral resonator, whose contour of the side surface follows an Archimedean spiral

with a small step [75–76, 116, 167–171]. This can be explained by the fact that such a shape does not depart far from a circle and thus may keep a low threshold of lasing, however is essentially non-symmetric to provide high directivity of emission.

In this Chapter, we consider the derivation of the Muller boundary integral equations as a tool for the analysis of electromagnetic field in the presence of a homogeneous dielectric object (in the 2-D formulation) with arbitrary smooth boundary. We also build an efficient numerical algorithm for their discretization, based on the interpolation using the quadrature formulas. Great attention is paid to the study of the convergence of this algorithm and the connection of the rate of convergence with the contour smoothness. The developed algorithm is applied to the investigation of the lasing frequencies and thresholds and also the fields of the H-polarized natural modes in a thin active resonator having a spiral shape. We study the removal of the mode degeneracy in terms of the frequency and threshold due to the appearance of the step on the contour. The mode fields in the near and far zones are also studied in detail.

5.1. Muller boundary integral equations

For either of two alternative polarizations, the reduction of the 2-D electromagnetic-filed eigenvalue problem to the boundary integral equations is based on the use of the Green's formulas. As mentioned in Chapter 1, only the Muller boundary integral equations possess the full equivalency to the original boundary-value problem for Maxwell equations with all additional conditions.

Geometry of a generic 2-D open dielectric resonator with a smooth contour and the used notations are shown in Fig. 5.1. We denote the outer domain as D_e, the inner domain as D_i, and the boundary of resonator as Γ. We will assume that $\dot{n}$ is the outer normal unit vector to the boundary Γ, and ν_j ($j = i, e$) are the refractive indices of the resonator material and the outer space, so that in the lasing eigenvalue problem $\nu_i = \alpha_i - i\gamma$ and $\nu_e = \alpha_e$.

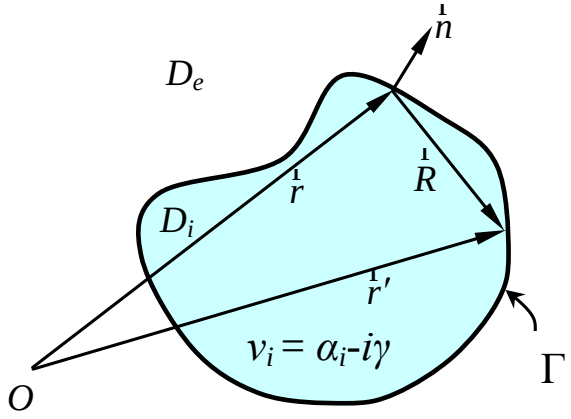

Fig. 5.1 Two-dimensional dielectric resonator of arbitrary shape

Suppose that the function U_j is the field component E_z or H_z, depending on the polarization, in the domains D_j, $j = i, e$ and solves the boundary-value problem,

$$\left(\Delta + k_{i,e}^2\right) U_{i,e}(\underset{1}{r}) = 0, \quad \underset{1}{r} \in D_i \cup D_e, \tag{5.1}$$

$$U_i\big|_\Gamma = U_e\big|_\Gamma; \quad \eta_i \frac{\partial U_i}{\partial n}\bigg|_\Gamma = \eta_e \frac{\partial U_e}{\partial n}\bigg|_\Gamma, \tag{5.2}$$

with the condition of local power finiteness and Sommerfeld condition of radiation (for U_e) at infinity, see (2.15). The coefficient in the equation (5.1) is defined in such a way that $k_{i,e} = k\nu_{i,e}$. The boundary conditions (5.2) follow from the demand that the tangential field components are continuous across Γ. Therefore the constants in (5.2) are defined as follows: $\eta_{i,e} = 1/\nu_{i,e}^2$ in the case of the H-polarization and $\eta_{i,e} = 1$ in the case of the E-polarization.

Introduce also the Green's function of the homogeneous medium, $G_j(\underset{1}{r}, \underset{1}{r'})$, which is the solution of the 2-D Helmholtz equation,

$$(\Delta + k_j^2) G_j(\underset{1}{r}, \underset{1}{r'}) = -\delta(\underset{1}{r}, \underset{1}{r'}), \tag{5.3}$$

with the Dirac delta-function $\delta(\underset{1}{r}, \underset{1}{r'})$ in the right-hand part. As known, the Green's function of a homogeneous medium having refractive index ν_i is

$$G_j(\vec{r},\vec{r}') = \frac{i}{4} H_0^{(1)}(k_j R), \tag{5.4}$$

where $R = |\vec{r} - \vec{r}'|$ is the distance between the points $\vec{r}$ and $\vec{r}'$, and $H_0^{(1)}(\cdot)$ is the Hankel function of the first kind and zero order.

Applying the second Green's formula to the functions $G_j(\vec{r},\vec{r}')$ and U_j, we obtain (see also [172], pp. 11 - 14):

$$U_i(\vec{r}) = -\int_\Gamma \left(U_i(\vec{r}') \frac{\partial G_i(\vec{r},\vec{r}')}{\partial n'} - G_i(\vec{r},\vec{r}') \frac{\partial U_i(\vec{r}')}{\partial n'} \right) dl', \quad \vec{r} \in D_i \tag{5.5}$$

$$U_e(\vec{r}) = \int_\Gamma \left(U_e(\vec{r}') \frac{\partial G_e(\vec{r},\vec{r}')}{\partial n'} - G_e(\vec{r},\vec{r}') \frac{\partial U_e(\vec{r}')}{\partial n'} \right) dl', \quad \vec{r} \in D_e, \tag{5.6}$$

where dl' is the element of the arc on Γ.

Denote $\varphi(\vec{r}) = U_i(\vec{r})$ and $\psi(\vec{r}) = \frac{\partial U_i(\vec{r})}{\partial n}$, $\vec{r} \in \Gamma$. Then from the boundary conditions (5.2) it follows that $U_e(\vec{r}) = \varphi(\vec{r})$ and $\frac{\partial U_e(\vec{r})}{\partial n} = \frac{\eta_i}{\eta_e} \psi(\vec{r})$, $\vec{r} \in \Gamma$. Further, in (5.5) and (5.6), move the point $\vec{r}$ to the contour Γ. Taking into account that the single-layer potential is continuous when crossing the boundary, we obtain

$$\frac{1}{2}\varphi(\vec{r}) = -\int_\Gamma \left(\varphi(\vec{r}') \frac{\partial G_i(\vec{r},\vec{r}')}{\partial n'} - G_i(\vec{r},\vec{r}') \psi(\vec{r}') \right) dl', \quad \vec{r} \in \Gamma, \tag{5.7}$$

$$\frac{1}{2}\varphi(\vec{r}) = \int_\Gamma \left(\varphi(\vec{r}') \frac{\partial G_e(\vec{r},\vec{r}')}{\partial n'} - \frac{\eta_i}{\eta_e} G_e(\vec{r},\vec{r}') \psi(\vec{r}') \right) dl', \quad \vec{r} \in \Gamma, \tag{5.8}$$

Adding (5.7) to (5.8), we arrive at the first integral equation,

$$\varphi(\vec{r}) + \int_{\Gamma} \varphi(\vec{r}')A(\vec{r},\vec{r}')dl' - \int_{\Gamma} \psi(\vec{r}')B(\vec{r},\vec{r}')dl' = 0. \qquad (5.9)$$

Move the point $\vec{r}$ in (5.5) and (5.6) to the contour Γ. On the differentiation of (5.5) and (5.6) in the normal $\vec{n}$ and taking into account the properties of the normal derivatives of the single and double-layer potentials, we obtain the expressions

$$\frac{1}{2}\psi(\vec{r}) = -\int_{\Gamma}\left(\varphi(\vec{r}')\frac{\partial^2 G_i(\vec{r},\vec{r}')}{\partial n'\partial n} - \psi(\vec{r}')\frac{\partial G_i(\vec{r},\vec{r}')}{\partial n}\right)dl', \quad \vec{r} \in \Gamma, \qquad (5.10)$$

$$\frac{\eta_i}{2\eta_e}\psi(\vec{r}) = \int_{\Gamma}\left(\varphi(\vec{r}')\frac{\partial^2 G_e(\vec{r},\vec{r}')}{\partial n'\partial n} - \frac{\eta_i}{\eta_e}\frac{\partial G_e(\vec{r},\vec{r}')}{\partial n}\psi(\vec{r}')\right)dl', \quad \vec{r} \in \Gamma. \qquad (5.11)$$

Addingя (5.10) to (5.11), we arrive at the second integral equation,

$$\frac{\eta_i + \eta_e}{2\eta_e}\psi(\vec{r}) + \int_{\Gamma} \varphi(\vec{r}')C(\vec{r},\vec{r}')dl' - \int_{\Gamma} \psi(\vec{r}')D(\vec{r},\vec{r}')dl' = 0. \qquad (5.12)$$

Equations (5.9) and (5.12) form the set of the Muller boundary integral equations. Here, the kernel functions are

$$A(\vec{r},\vec{r}') = \frac{\partial G_i(\vec{r},\vec{r}')}{\partial n'} - \frac{\partial G_e(\vec{r},\vec{r}')}{\partial n'}, \qquad (5.13)$$

$$B(\vec{r},\vec{r}') = G_i(\vec{r},\vec{r}') - \frac{\eta_i}{\eta_e}G_e(\vec{r},\vec{r}'), \qquad (5.14)$$

$$C(\vec{r},\vec{r}') = \frac{\partial^2 G_i(\vec{r},\vec{r}')}{\partial n\partial n'} - \frac{\partial^2 G_e(\vec{r},\vec{r}')}{\partial n\partial n'}, \qquad (5.15)$$

$$D(\vec{r},\vec{r}') = \frac{\partial G_i(\vec{r},\vec{r}')}{\partial n} - \frac{\eta_i}{\eta_e}\frac{\partial G_e(\vec{r},\vec{r}')}{\partial n}, \tag{5.16}$$

The Green's functions are defined according to (5.4) and their normal derivatives are calculated after the following expressions:

$$\frac{\partial G_j(\vec{r},\vec{r}')}{\partial n'} = (i/4)k_j H_1^{(1)}(k_j R)(\vec{R}\cdot\vec{n}')/R \tag{5.17}$$

$$\frac{\partial G_j(\vec{r},\vec{r}')}{\partial n} = (-i/4)k_j H_1^{(1)}(k_j R)(\vec{R}\cdot\vec{n})/R \tag{5.18}$$

$$\frac{\partial^2 G_j(\vec{r},\vec{r}')}{\partial n\partial n'} = -\frac{ik_j}{4}\left[k_j H_2^{(1)}(k_j R)(\vec{R}\cdot\vec{n}')\frac{(\vec{R}\cdot\vec{n})}{R^2} - H_1^{(1)}(k_j R)\frac{(\vec{n}'\cdot\vec{n})}{R}\right] \tag{5.19}$$

In (5.17) – (5.19), the quantities $(\vec{R}\cdot\vec{n})$, $(\vec{R}\cdot\vec{n}')$ and $(\vec{n}'\cdot\vec{n})$ are the scalar products of the corresponding vectors. Assume that the contour Γ parameterization is performed with the aid of the function $r(t) = \{x(t), y(t)\}$. Then the distance between two points on the contour is given by the expression

$$R = \sqrt{\left[x(t) - x(\tau)\right]^2 + \left[y(t) - y(\tau)\right]^2}, \tag{5.20}$$

and the outer normal unit vector to the boundary is given by the expression

$$\vec{n} = \left(\frac{dy}{dt}; -\frac{dx}{dt}\right)\frac{1}{L(t)}, \tag{5.21}$$

where $L(t)$ is the Jacobian,

$$L(t) = \sqrt{(dx/dt)^2 + (dy/dt)^2}\,. \qquad (5.22)$$

Thus, the kernels of the Muller equations are the linear combinations of the Green's functions of the homogeneous media having parameters of the outer and inner media, and their normal derivatives of the first and second order. Consider the properties of the kernels (5.13) – (5.16) at $t \to \tau$. By definition, the Hankel function is $H_n^{(1)}(z) = J_n(z) + iY_n(z)$, and the Bessel and Neumann functions can be presented as (see [156]):

$$J_n(z) = \sum_{p=0}^{\infty} \frac{(-1)^p}{p!(n+p)!}\left(\frac{z}{2}\right)^{n+2p} \qquad (5.23)$$

$$\begin{aligned} Y_n(z) = {} & \frac{2}{\pi}\left[\ln\frac{z}{2} + C\right] J_n(z) - \frac{1}{\pi}\sum_{p=0}^{n-1}\frac{(n-1-p)!}{p!}\left(\frac{2}{z}\right)^{n-2p} \\ & -\frac{1}{\pi}\sum_{p=0}^{\infty}\frac{(-1)^p}{(n+p)!}\left(\frac{z}{2}\right)^{n+2p}\{\phi(p+n)+\phi(p)\}, \end{aligned} \qquad (5.24)$$

where $\phi(0) = 0, \quad \phi(p) = \sum_{m=1}^{p}\frac{1}{p}, \quad p = 1,2,...,$ and $C = 0.5772157...$ is Euler's constant. If $n = 0$, finite sum in (5.24) turns zero.

From the expansions (5.23) and (5.24), we find that the kernel functions $A(t,\tau)$ in (5.13) and $D(t,\tau)$ in (5.16) arte continuous at all points of a smooth contour, and the kernel functions $B(t,\tau)$ in (5.14) and $C(t,\tau)$ in (5.15) have logarithmic singularities. Note that the kernel $B(t,\tau)$ is singular only in the case of the H-polarization; in the case of the E-polarization it is continuous. The continuity of the kernel functions $A(t,\tau)$ and $D(t,\tau)$ is conditioned by the following property (see, for instance, [173] p. 346)

$$\frac{\partial G_j(t,t)}{\partial n} = \frac{1}{2}\chi_0(t), \tag{5.25}$$

where $\chi_0(t)$ is the curvature (see [174], p. 53) of the contour Γ at the point $\overset{1}{r}$.

The limiting behavior of two kernel functions that are singular at $t \to \tau$, has the following form::

$$B(t,\tau) \underset{t\to\tau}{\cong} -\frac{1}{2\pi}\left(1-\frac{\eta_i}{\eta_e}\right)\ln R \tag{5.26}$$

$$C(t,\tau) \underset{t\to\tau}{\cong} -\frac{1}{2\pi}\left(k_i^2 - k_e^2\right)\ln R. \tag{5.27}$$

5.2. Integral equations discretization using the quadratures

As mentioned, there are several ways of efficient discretization of the boundary integral equations. For instance, this can be done with the aid of simple collocations or Galerkin projection method that have been applied to the Muller equation in [121] and [122], respectively. Besides of the mentioned, one of the most efficient discretization techniques is the method of quadratures also known as Nystrom method [125, 175, 176].

This discretization method is based on the replacement of the integrals with approximate sums using the appropriate quadrature formulas. Therefore the center of gravity in the development of corresponding numerical algorithms is placed on the derivation of the quadrature formulas that correctly take into account the behavior of the integrand functions, and first of all their possible singularities.

In this Chapter, we will consider the discretization of integral equations with closed contours of integration that admit a regular analytical 2π-periodic parameterization with the aid of function $\mathrm{r}(t) = \{x(t), y(t)\}$, $t \in [0, 2\pi]$. As some of

the kernel functions have logarithmic singularities, it is convenient to represent all of the kernels (5.13) – (5.16) in such a way that these singularities are extracted; such a decomposition can be done for the smooth kernels as well:

$$A(t,\tau) = A_1(t,\tau)\ln\left[4\sin^2\frac{t-\tau}{2}\right] + A_2(t,\tau),$$

$$B(t,\tau) = B_1(t,\tau)\ln\left[4\sin^2\frac{t-\tau}{2}\right] + B_2(t,\tau),$$

$$C(t,\tau) = C_1(t,\tau)\ln\left[4\sin^2\frac{t-\tau}{2}\right] + C_2(t,\tau), \qquad (5.28)$$

$$D(t,\tau) = D_1(t,\tau)\ln\left[4\sin^2\frac{t-\tau}{2}\right] + D_2(t,\tau),$$

where $A_1(t,\tau)$, $B_1(t,\tau)$, $C_1(t,\tau)$ and $D_1(t,\tau)$ are the analytic functions defined as follows:

$$A_1(t,\tau) = (-1/4\pi)\left[k_i J_1(k_i R) - k_e J_1(k_e R)\right](\vec{R}\cdot\vec{n}')/R,$$

$$B_1(t,\tau) = (-1/4\pi)\left[J_0(k_i R) - (\eta_i/\eta_e)J_0(k_e R)\right],$$

$$C_1(t,\tau) = (1/4\pi)\left[k_i^2 J_2(k_i R) - k_e^2 J_2(k_e R)\right](\vec{R}\cdot\vec{n}')(\vec{R}\cdot\vec{n})/R^2 - \qquad (5.29)$$

$$(1/4\pi)\left[k_i J_1(k_i R) - k_e J_1(k_e R)\right](\vec{n}'\cdot\vec{n})/R,$$

$$D_1(t,\tau) = (1/4\pi)\left[k_i J_1(k_i R) - (\eta_i/\eta_e)k_e J_1(k_e R)\right](\vec{R}\cdot\vec{n})/R$$

The functions $A_2(t,\tau)$, $B_2(t,\tau)$, $C_2(t,\tau)$, $D_2(t,\tau)$ are found from (5.28) with account of (5.29). Further, we introduce an equidistant mesh of nods on the

contour Γ at $t_p = \pi p / N$, $p = 0,1,...,2N-1$. The integrals of the each part of kernels are replaced with the sums using the quadrature formulas. For the logarithmic parts we use the quadrature formula derived through the approximation of the integrand function with trigonometric polynomials [125, 175, 176],

$$\int_0^{2\pi} \ln\left[4\sin^2\frac{t-\tau}{2}\right] F_1(t,\tau) f(\tau) L(\tau) d\tau \approx \sum_{p=0}^{2N-1} P_p^{(N)}(t) F_1(t,t_p) f(t_p) L(t_p), \qquad (5.30)$$

where the trigonometric polynomial has the form as

$$P_p^{(N)}(t) = -(2\pi/N)\sum_{m=1}^{N-1} \cos\left[m(t-t_p)\right]/m - \pi\cos\left[N(t-t_p)\right]/N^2 \qquad (5.31)$$

For the other, continuous parts of kernels we use the trapezoidal rule ([125, 156])

$$\int_0^{2\pi} F_2(t,\tau) f(\tau) L(\tau) d\tau \approx (\pi/N)\sum_{p=0}^{2N-1} F_2(t,t_p) f(t_p) L(t_p) \qquad (5.32)$$

In the formulas (5.30) and (5.32), it is implied that $F_1 = A_1, B_1, C_1, D_1$; and $F_2 = A_2, B_2, C_2, D_2$, and also $f = \varphi, \psi$.

In order to obtain the values of the parts of kernels in (5.28) at $t = \tau$, we make use of the expansions (5.23) and (5.24). Then, for the first parts we have

$$\begin{aligned} &A_1(t,t) = 0; \quad B_1(t,t) = -\left(1-\eta_i/\eta_e\right)/4\pi, \\ &C_1(t,t) = -\left(k_i^2 - k_e^2\right)/8\pi; \quad D_1(t,t) = 0, \end{aligned} \qquad (5.33)$$

and for the second parts we obtain

$$A_2(t,t)=0,\quad D_2(t,t)=-\left(1-\eta_i/\eta_e\right)\chi_0\left(t\right)/4\pi,$$

$$B_2(t,t)=\left(1-\eta_i/\eta_e\right)\left(i\pi-2C-\ln L^2(t)\right)/4\pi+\left(\ln\frac{4}{k_i^2}-(\eta_i/\eta_e)\ln\frac{4}{k_e^2}\right)/4\pi,$$

$$C_2(t,t)=\left(k_i^2-k_e^2\right)\left(i\pi-2C+1\right)/8\pi+\left(k_i^2\ln\frac{4}{k_i^2}L^2(t)-k_e^2\ln\frac{4}{k_e^2}L^2(t)\right)/8\pi \tag{5.34}$$

On the substitution, in the integral equations (5.9) and (5.12), the integrals with the quadratures (5.30) and (5.32), we arrive at the following matrix equation of the size $4N\times 4N$

$$\left[\mathbf{I}+\mathbf{A}\right]\begin{pmatrix}\Phi\\ \Psi\end{pmatrix}=0, \tag{5.35}$$

where the vectors of unknowns are $\Phi=\left\{\varphi(t_p)\right\}_{p=0,2N-1}$ and $\Psi=\left\{\psi(t_p)\right\}_{p=0,2N-1}$, and the matrix $\mathbf{A}$ has the block structure,

$$\mathbf{A}=\begin{bmatrix}A & -B\\ C & -D\end{bmatrix} \tag{5.36}$$

Every block has the size of $2N\times 2N$ and its elements are given by

$$A=\left\{(P_p^{(N)}(t_s)A_1(t_s,t_p)+(\pi/N)A_2(t_s,t_p))L(t_p)\right\}_{p,s=0}^{2N-1},$$

$$B=\left\{2\eta_e/(\eta_e+\eta_i)(P_p^{(N)}(t_s)B_1(t_s,t_p)+(\pi/N)B_2(t_s,t_p))L(t_p)\right\}_{p,s=0}^{2N-1},$$

$$C=\left\{(P_p^{(N)}(t_s)C_1(t_s,t_p)+(\pi/N)C_2(t_s,t_p))L(t_p)\right\}_{p,s=0}^{2N-1}, \tag{5.37}$$

$$D=\left\{2\eta_e/(\eta_e+\eta_i)(P_p^{(N)}(t_s)D_1(t_s,t_p)+(\pi/N)D_2(t_s,t_p))L(t_p)\right\}_{p,s=0}^{2N-1}$$

Thus, the lasing eigenvalues (κ,γ) are the roots of determinantal equation,

$$\det\left[\mathbf{I}+\mathbf{A}(k,\gamma)\right]=0 \qquad (5.38)$$

Considering the accuracy of computations, we can note that if the integrand function is analytic and 2π-periodic, then, according to [125], the error associated with (5.31) and (5.32) has the order of $O\left[\exp(-\sigma N)\right]$, where $2N$ is the number of nods in the quadrature and σ is the half-width of the strip in the complex plane where the integrand functions $F_{1,2}(t,\tau)f(\tau)L(\tau)$ can be continued holomorphically. Two examples of the real-life behavior of the computational errors for the eigenvalues in the case of a spiral resonator is shown in Fig. 5.2 as a function of N.

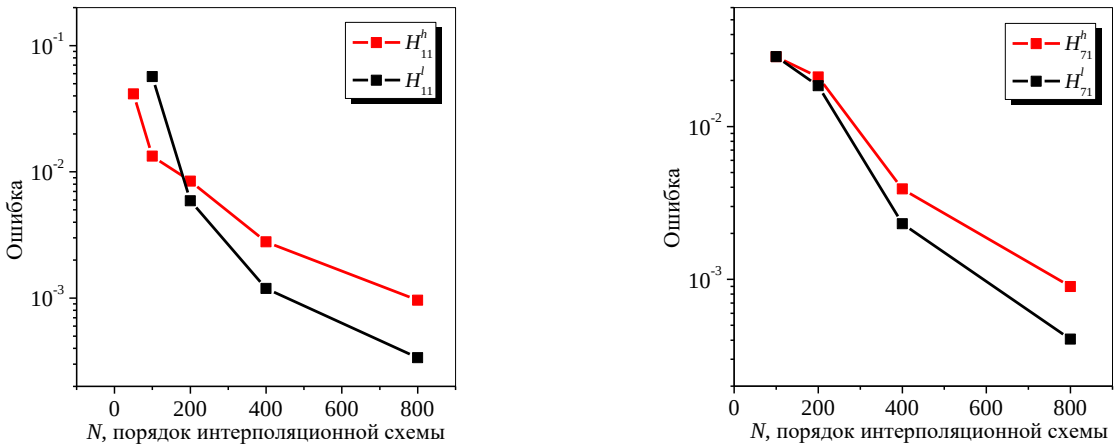

(a) (b)

Fig. 5.2 Computational errors associated with the lasing eigenvalues for two doublets of the dipole-type and whispering-gallery modes in a spiral resonator, as a function of the order of interpolation scheme. Modes $H_{1,1}^{h,l}$ (a) and modes $H_{7,1}^{h,l}$ (b), resonator parameters are d = 1.0a, $\beta=\pi/100$ (see section 5. 3), α_i=2.63, α_e=1

Relaxation of the requirements to the smoothness of the integrand functions leads to smaller rates of convergence of the algorithm. For example, the error of the quadrature formula (5.30) amounts $O(C/N^{r+\varepsilon})$, $C=const$ under the assumption

that that the function factor at the logarithm belongs to the class of Holder-continuous functions, $C^{r,\varepsilon}$ (i.e., r times continuously differentiable, with the r-the derivative satisfying the Holder condition with index $\varepsilon \in (0,1]$) (see [176]). In (5.32), the error of approximation for the 2π-periodic functions of the class C^r (i.e., r times continuously differentiable functions) has the order of $O(C/N^r)$, $C = const$ (see. [156] for details).

The roots (κ, γ) of the approximate determinantal equation, as before, are found numerically using the iterative-type secant method. In the process of computations, the accuracy of determining the roots has been fixed at the level of 10^{-7}. The number of iterations strongly depends on the nearness of initial guess to the true eigenvalue.

5.3. Modes of an active resonator with a spiral contour

In this section, we present the numerical study of the H-polarized lasing modes of a 2-D uniformly active spiral depicted in Fig. 5.3. We can consider the spiral contour as a slightly deformed in asymmetric manner circular resonator, therefore we will, in fact, study the effect of the perturbation of this contour on the spectrum of lasing frequencies and associated thresholds, and also on the directionality of the emission.

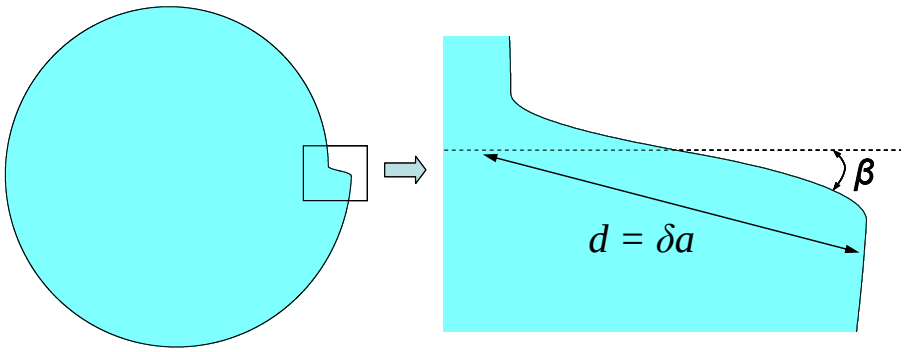

Fig. 5.3 Geometry of a spiral resonator with a smoothed step whose contour is characterized with the function (5.39)

The numerical results presented below have been obtained for the lowest-order lasing modes: perturbed monopole-type mode $H_{0,1}$, dipole-type modes $H_{1,1}$, and quadruple-type modes $H_{2,1}$ мод, and also the quasi-whispering-gallery modes that are the perturbations of the mode $H_{7,1}$. We have not performed the simulations for the whispering-gallery mode of very high azimuth indices. This is explained by the limitations imposed by the moderate smoothness of the contour parameterization used here and also by the properties of the quadrature formulas. However the mentioned limitations are conditional and can be lifted using several approaches that can be a subject of a separate study.

At the same time, the lowest-order modes in a spiral resonator are of considerable interest themselves because, as discussed in section 4.3, the thresholds of lasing of such modes can be considerably lowered by collecting several resonators into a cyclic photonic molecule.

For the parameterization of the spiral contour, we have chosen the following piece-wise function proposed originally in [177]:

$$\begin{cases} x(t) = r(t)\cos t \\ y(t) = r(t)\sin t \end{cases}, \quad t \in [0, 2\pi], \tag{5.39}$$

where

$$r(t) = \begin{cases} 1 + \delta / 4\pi t, & t \in [\beta, 2\pi - \beta] \\ 1 - \delta / 4\pi \left[t(2\pi - \beta)/\beta - t^2 \pi / \beta^2 - \pi \right], & t \in [0, \beta) \\ 1 + \delta / 4\pi \left[(2\pi - t)(2\pi - \beta)/\beta - (2\pi - t)^2 \pi / \beta^2 + \pi \right], & t \in (2\pi - \beta, 2\pi], \end{cases} \tag{5.40}$$

a is the minimum radius of the resonator, and $d = \delta a$ is the height of the step on the contour of spiral resonator, and β is the angle of step inclination counted from the horizontal direction.

With this parameterization of the spiral contour, we obtain a smooth curve, however its second derivative $r''(t)$ has two finite jumps at $t = \beta$ and $t = 2\pi - \beta$. As

the functions $x(t)$ and $y(t)$ from (5.39) appear in the kernels of integral equations (5.9) and (5.12), then the integrand functions $F_{1,2}(t,\tau)\,f(\tau)L(\tau)\in C[0,2\pi]$. Moreover, the used parameterization formula (5.39)-(5.40) is not a 2π-periodic one. Nevertheless, using the formulas (5.39), (5.40), one can still obtain a number of important results as it provides the convergence of algorithm, although not rapid.

The monopole, dipole, and quadruple modes of circular and, as a consequence, of the slightly perturbed circular resonators have high thresholds of lasing. The can be found numerically, for instance with the accuracy of up to 3 digits and within a few hours of computation time on a moderate desktop computer, by using (5.40) and quadratures (5.30), (5.32) with a relatively moderate number of nods. For the whispering-gallery modes withy the azimuth indices $m>10$, the thresholds are very low and one faces the difficulty of computation of eigenvalues with much finer accuracy. In this case, the parameterization with (5.40) is inefficient in view of not sufficient smoothness.

Note also that in the parameterization formula, the parameter β is involved, responsible for the inclination of the step in the spiral contour. Therefore at the discretization the distance between the adjacent nods should be kept smaller than β. If the mesh of nods is equidistant, then very small values of β entail very large number of nods and correspondingly large computation time, thus making the computational scheme inefficient (although still convergent). As a remedy, one should use a non-equidistant mesh of nods that get denser around the step or apply a parameterization with the aid of the arc of the curve. Both of these options will require the use of different quadrature formulas.

To find good initial guesses for a quick search of roots of (5.38), we have built the relief of the absolute value of determinant on the plane (κ,γ). In Fig. 5.4, presented is such a relief for a resonator with parameters $\delta=2a,\ \ \beta=\pi/100$ and effective refractive index $\alpha_i=2.63$, computed using the scheme with the number of nods $N=100$. On this relief, one can see several deep minima. All minima, except of the first, the lowest, in frequency, correspond to the closely located pairs of modes

(eigenvalues). Each pair of these modes originates from the "former" double degenerate mode $H_{m,n}$, $m>0$ of the circular resonator that is split now in the doublet due to the removal of degeneracy caused by the loss of rotational symmetry. The first, solitary, minimum corresponds to the monopole mode of the spiral resonator, $H_{0,1}$, which originates from the non-degenerate monopole mode of the circle.

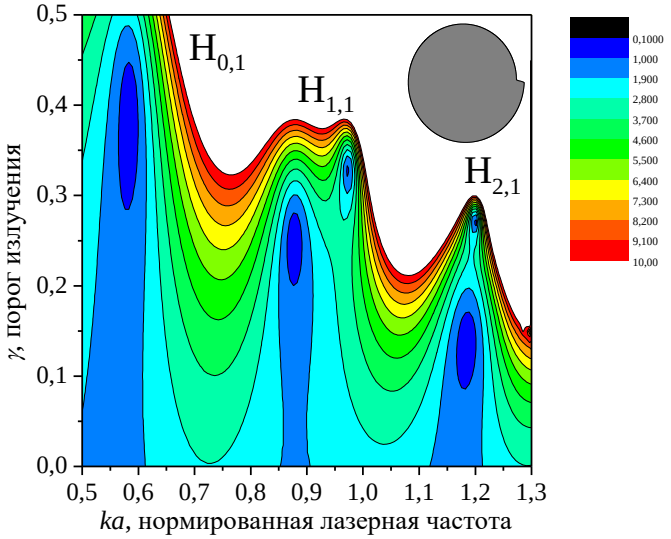

Fig. 5.4 Equal-value lines of the absolute value of determinant (5.38) as a function of two variables, (ka,γ), $d=2a$, $\beta=\pi/100$, $N=100$, $\alpha_i=2.63$

In Figs. 5.5 - 5.8, presented are the dependences of the lasing frequencies and thresholds of the modes of the doublets $H_{1,1}^{h,l}$ and $H_{2,1}^{h,l}$ on the normalized step height of a spiral resonator d/a (if $d=0$ the contour transforms into the circle).

The doublets are formed by the modes that are close to each other in frequency but with a lower and a higher value of thresholds. Therefore we denote these sister-modes as $H_{m,n}^{h,l}$, where two lower integer indices, similarly to the circular resonator, characterize (now conditionally) the numbers of field variations in azimuth and in radius, respectively, and the lower index corresponds to the value of the lasing

threshold of the given mode. Thus, a mode with a higher threshold obtains the index h and a sister-mode with a lower threshold obtains the index l.

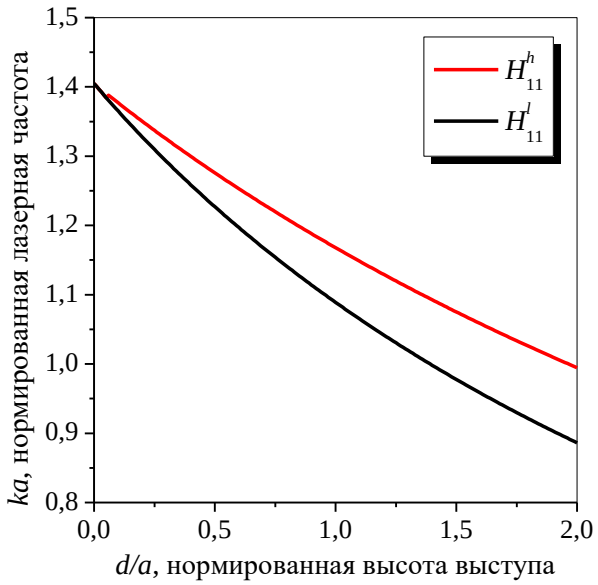

Fig. 5.5 Dependences of the lasing frequencies on the normalized step height in spiral resonator, for the modes of the doublet $H_{1,1}^{h,l}$, $\beta = \pi/100$, $N = 200$, $\alpha_i = 2.63$, $\alpha_e = 1$

The most interesting finding is that the threshold of one of the lowest modes in a doublet gets smaller with the growth of the step (see Figs. 5.6 and 5.8).

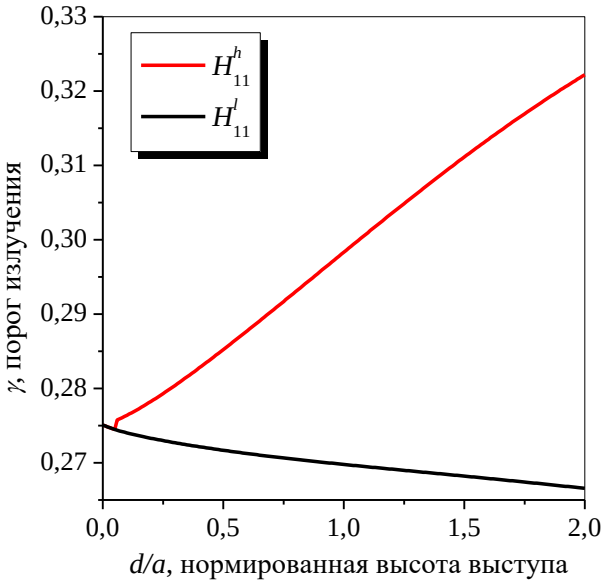

Fig. 5.6 The same as in Fig. 5.5 however for the lasing thresholds.

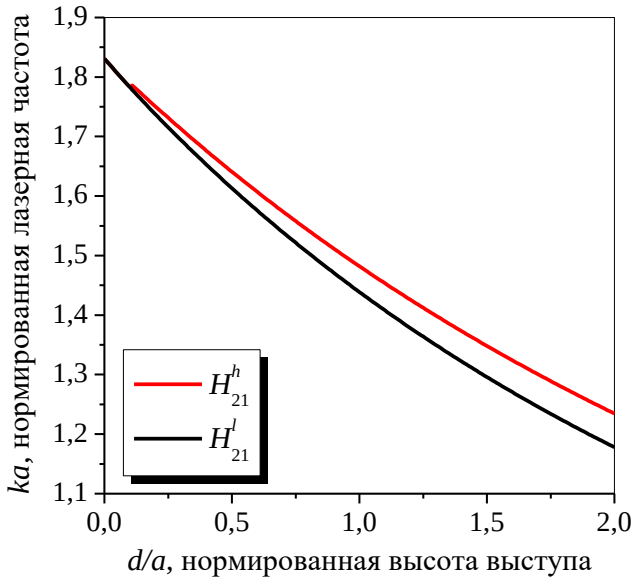

Fig. 5.7 The same as in Fig. 5.5 however for the modes of the doublet $H_{2,1}^{h,l}$

Our algorithm tends to find only one of them if the distance between the eigenvalues gets smaller than the accuracy provided by the contour parameterization and the number of nods applied, at the expense of the greater time of computations.

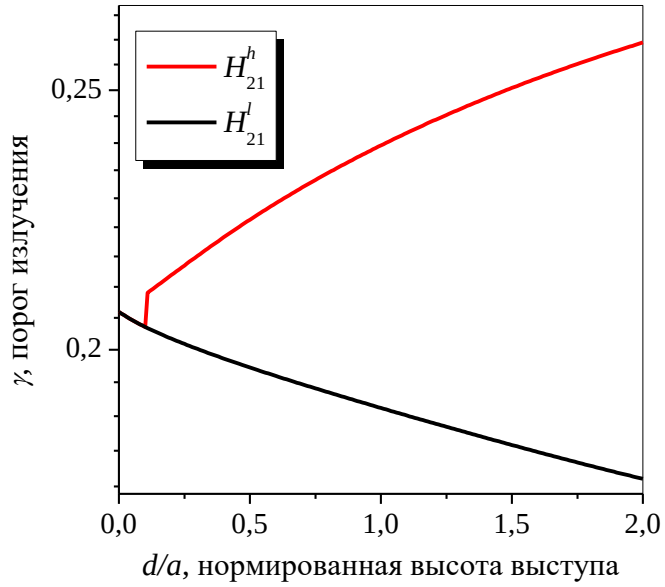

Fig. 5.8 The same as in Fig. 5.7 however for the lasing thresholds

In Fig. 5.9, we show the amplitude near-field and far-field patterns for the modes $H_{0,1}$, $H_{1,1}^{h,l}$ and $H_{2,1}^{h,l}$ in the spiral resonator with $d = 0.3a$ and $\beta = \pi/100$.

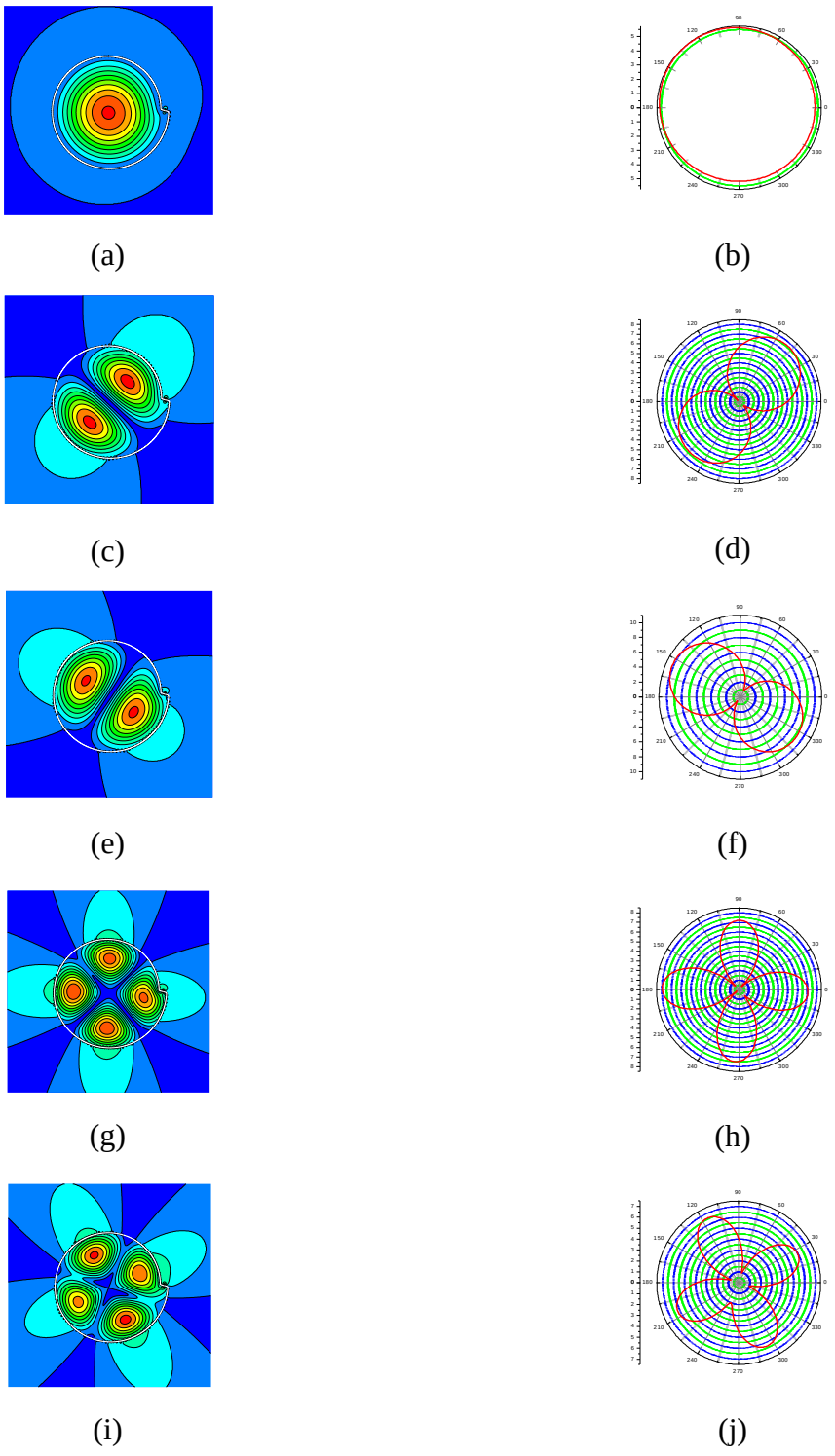

Fig. 5.9 Near and far fields, $|H_z|$, of the modes in a spiral resonator: $H_{0,1}$ (a), (b) *ka* = 0.82, $\gamma = 0.35$; $H^h_{1,1}$ (c), (d) *ka* = 1.32, $\gamma = 0.28$; $H^l_{1,1}$ (e), (f) *ka* = 1.29, $\gamma = 0.26$; $H^l_{2,1}$, (g), (h) *ka* = 1.69, $\gamma = 0.18$; $H^h_{2,1}$ (i), (j) *ka* = 1,7, $\gamma = 0.21$. Parameters of the contour are $d = 0.3a$, $\beta = \pi/100$, $\alpha_i = 2.63$, $\alpha_e = 1$, number of nods is $N = 100$

Far-field expression for the mode field can be obtained using the asymptotic of the Hankel function for the large argument (see [156]) and representation (5.6). It results in the following formula:

$$U_e(r,\theta)\underset{r\to\infty}{=}-\frac{i+1}{4\sqrt{\pi k_e r}}e^{ik_e r}\int_\Gamma\left[i\varphi k_e\left(\vec{n}'\cdot(\cos\theta,\sin\theta)\right)+\frac{\eta_i}{\eta_e}\psi\right]e^{-ik_e\left(\vec{r}'\cdot(\cos\theta,\sin\theta)\right)}dl', \qquad (5.41)$$

where θ is the angle of observation.

Our analysis has shown that for the lowest-order modes the appearance of the step on the contour has practically no effect on the directivity of emission with respect to the radiation from the circular resonator: it remains close to 2.

In Figs. 5.10 and 5.11, presented are the dependences of the lasing frequencies and thresholds on the normalized step height for the whispering-gallery mode of the doublet $H_{7,1}^{h,l}$. Here, the step inclination angle is $\beta=\pi/100$ and the number of nods in the quadrature formula is $2N=800$.

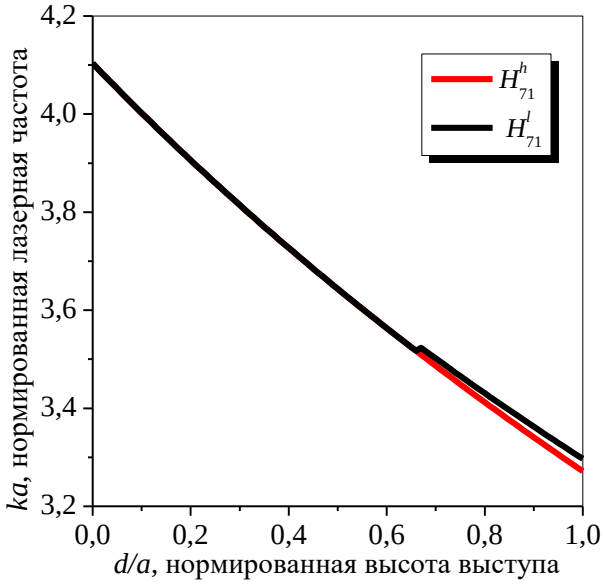

Fig. 5.10 Dependences of the lasing frequencies on the normalized step height in spiral resonator, for the modes of the doublet $H_{7,1}^{h,l}$, the other parameters are $\beta=\pi/100,\ N=400,\ \alpha_i=2.63,\ \alpha_e=1$

Similarly to the dipole modes, the whispering-gallery mode $H_{7,1}$ displays the splitting into a doublet caused by the removal of degeneracy by the step on the contour and loss of rotational symmetry. However a noticeable splitting is observed only if the step is considerable, $d > 0.6a$.

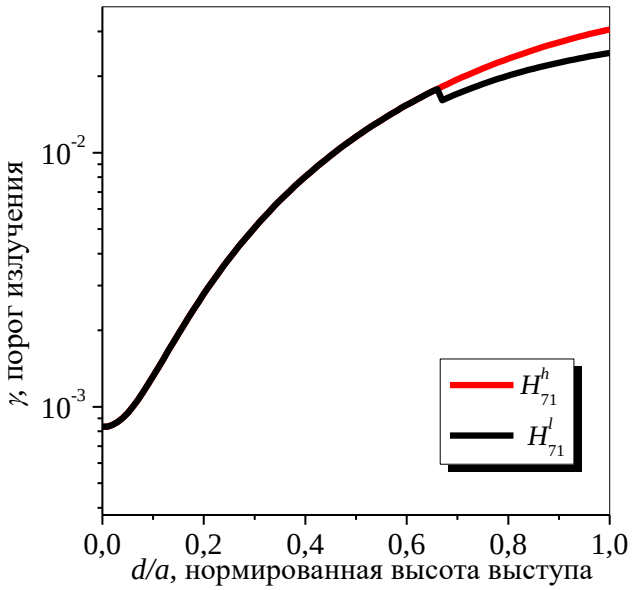

Fig. 5.11 The same as in Fig. 5.10 however for the lasing thresholds.

If the step height decreases, the modes of the doublet merge together and their thresholds tend to the ultra-low value characteristic for the mode $H_{7,1}$ of the circle. The same tendency is seen for the frequencies of lasing (see Figs. 5. 10 and 5. 11). Note that a large step ($d = 1.0a$) in the spiral resonator leads to the growth of thresholds of the both modes of that doublet by an order of magnitude with respect to the same mode in the active circular dielectric resonator.

The main difference in the dynamics of mode thresholds as a function of the step height, between the lower-order and the whispering-gallery modes, is that for the latter modes, there is no reduction of threshold at all. Both mode thresholds grow quickly in Fig. 5.11 unlike one of the thresholds in Figs. 5.6 and 5.8.

The near and far field patterns $|H_z|$ for the whispering-gallery modes $H_{7,1}^{h,l}$ in a spiral resonator are presented in Fig. 5. 12; here the step height is equal to the minimum radius, $d = 1.0a$.

As visible, the presence of the step removes the degeneracy however considerably distorts the patterns of the whispering-gallery modes (compare with results of section 2). In the far zone, the patterns of emission for the both modes of this doublet, $H_{7,1}^{h,l}$, have several well shaped main beams (see Figs. 5.12 (b), (d)), in contrast to the 2m identical beams for the circular resonator (see Figs. 2.10 in section 2.3).

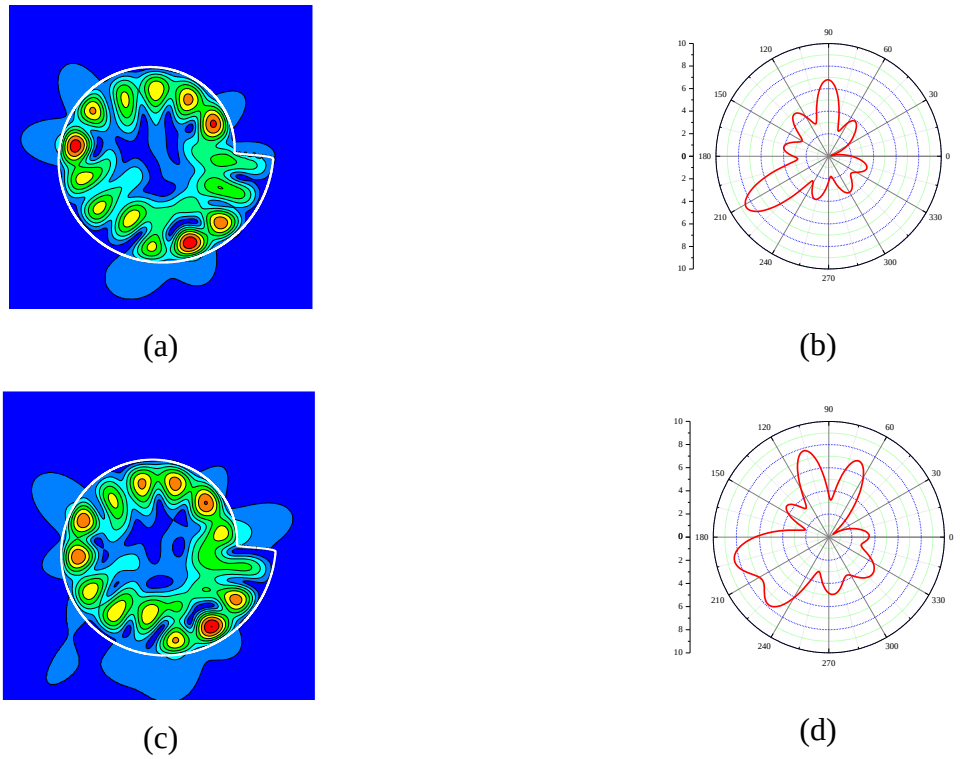

Fig. 5.12 Near and far fields $|H_z|$ for the whispering-gallery modes of the doublet $H_{7,1}^{l,h}$ in a spiral resonator with a large step: $H_{7,1}^{l}$ (a), (b): ka = 3.2962, γ = 2. 52*10^{-2}; N=400; $H_{7,1}^{h}$(c), (d): ka = 3.2714, γ = 3.048*10^{-2}, N=400. Other parameters are d = 1.0a, $\beta = \pi/100$, α_i=2.63, α_e=1

For the modes of the higher azimuth orders, the computation of similar dependences of the frequencies and thresholds on the step height needs a larger time because of the larger accuracy of the quadrature formulas requiring a larger number of nods.

CONCLUSIONS FOR CHAPTER 5

In this Chapter, we have considered 2-D model of the uniformly active dielectric open resonator with a smooth contour and interpolation-type method of its reduction to the determinantal equation. Further we have performed a systematic numerical analysis of the lasing frequencies and thresholds, and also the modal fields for the resonator shaped as a spiral. The results of these studies have been published in a journal paper [7] and conference proceedings [42–43, 46]; they enable us to make the following conclusions:

1. The Nystrom method with the separation of the logarithmic parts in the kernels of the Muller integral equations allows to build an exponentially convergent numerical algorithm of computation of the lasing eigenvalues (frequencies and thresholds of lasing) for a 2-D resonator with analytic (i.e. infinitely differentiable) contour.

2. In the case of the contour parameterization given in piece-analytic manner, this method enables one to achieve an algebraic convergence, with the rate of convergence depending on the number of continuous derivatives of the function, which parameterizes the contour.

3. When looking numerically for the eigenvalues, convenient initial guesses can be found by taking the minima on relieves of the absolute values of the determinants of the discretized integral equations as a function of two parameters, frequency and threshold of lasing.

4. Smooth parameterization of the spiral contour with the aid of function (5.40) enables one to compute the lasing eigenvalues for the modes with the azimuth number $m<10$ with accuracy to 3-4 digits within the time measures in minutes and hours on a moderate desktop computer.

3. In the spiral resonator, the presence of a step on the contour leads to the removal of degeneracy of the formerly degenerate modes (except of the monopole mode) and appearance of doublets.

4. The lowest H-polarized modes in the spiral resonator (monopole, dipole and quadruple modes) are weakly perturbed by the step on the contour even if the step height is large and comparable to the radius of non-perturbed resonator. This is explained by the fact that the fields of these modes are not confined at the rim of the resonator but distributed over its whole volume. If the step is small, then the threshold of one of the modes of the lowest doublets obtains lower value than in the circular counterpart. The directivity of emission of the perturbed lowest modes in the far zone remains close to 2.

5. Higher-order modes of the spiral resonators are the perturbations of the whispering-gallery modes whose fields are confined at the rim of the resonator. Therefore the appearance of the step on the contour perturbs them stronger. Here, the both mode thresholds rapidly grow up if the step height gets larger and increase by an order of magnitude for the modes of the doublet $H_{7,1}^{h,l}$ in a GaAs resonator if the step makes a half of the cavity minimum radius. The directivities of these modes increase to 5-6 because of formation of one or two well-shaped main beams of emission in the far zone.